PROCEEDINGS OF SCIENCE

Simulating radio emissions from particle showers in complex media with CORSIKA 8

Philipp Windischhofer[a,*] **and Alan Coleman**[b] **for the CORSIKA 8 Collaboration**
(a complete list of authors can be found at the end of the proceedings)

[a] *Dept. of Physics, Enrico Fermi Institute, Kavli Institute for Cosmological Physics, University of Chicago, Chicago, IL 60637*
[b] *Department of Physics and Astronomy, Uppsala University, Uppsala, Sweden*

E-mail: windischhofer@uchicago.edu

CORSIKA 8 is a modern Monte-Carlo simulation framework for particle showers in air and dense media. The calculation of shower-induced radio-emissions is a key element of the code, relevant for experiments targeting radio detection of cosmic rays and neutrinos, among others. In this contribution, we report on the unique capabilities of CORSIKA 8 to simulate the radio emission from showers developing in inhomogeneous media and the propagation of this radiation through these complex environments that cannot be properly treated with other methods. Several radio emission and propagation algorithms are provided by the framework, including the *Endpoint* and *ZHS* formalisms, numerical raytracing, and a new Green's function-based approach for a full-electrodynamics signal calculation provided by the *Eisvogel* package. We briefly review these approaches and show simulation results relevant for radio neutrino experiments operating in the Arctic and Antarctic, including the modeling of in-ice particle cascades and the characterization of the physics background arising from cosmic-ray air shower cores impacting the ice sheet.

39th International Cosmic Ray Conference (ICRC2025)
15–24 July 2025
Geneva, Switzerland

ICRC 2025
The Astroparticle Physics Conference
Geneva July 15-24, 2025

*Speaker

PoS(ICRC2025)1214

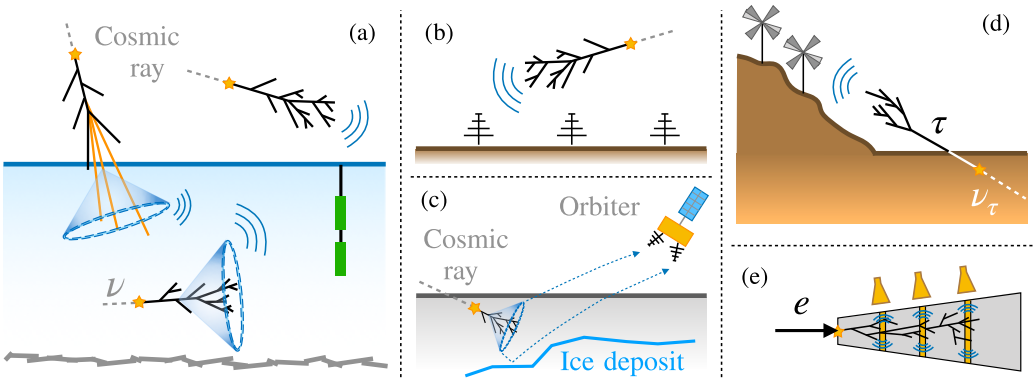

Figure 1: Illustration of radio particle detection experiments being considered or already in operation for which radio propagation through complex environments plays an important role: (a) in-ice neutrino observatory with cosmic rays as important backgrounds, (b) radio detection of highly-inclined air showers, (c) search for sub-surface lunar ice deposits, (d) radio detection of upgoing tau neutrinos, (e) radio calorimeter. The first interaction of the primary particle is marked by a yellow star.

1. Introduction

A growing number of experiments are using broadband radio receivers to detect interactions of high-energy particles as probes of fundamental physical processes. In many cases, these experiments instrument large volumes of naturally-occurring media—such as glacial ice or lunar regolith—and receivers are therefore placed in spatially inhomogeneous materials or near dielectric boundaries. Fig. 1 shows several examples. For in-ice neutrino observatories such as RNO-G [1] or ARA [2], cosmic ray air showers form a main physics background (Fig. 1a). Spatially localized radiation propagation modes such as atmospheric ducting may also play a role in the radio detection of highly-inclined air showers (Fig. 1b), while reflection of Askaryan radiation on internal material layers forms the basis for the CoRaLs project [3] to search for sub-surface ice deposits in the permanently-shadowed regions of the moon (Fig. 1c). Elevated antennas are being explored by the TAROGE-M [4], BEACON [5] and GRAND [6] collaborations for the detection of upgoing hadronic cascades from tau neutrinos, involving radiation wavefronts propagating near (or along) the surface (Fig. 1d). Finally, radio calorimeters [7] may form a promising detector technology for future energy-frontier particle collider experiments (Fig. 1e).

To fully exploit the physics potential of each of these experiments, it is important to model the radio emission from particle cascades and the propagation of this radiation through complex media at high fidelity. In the following, we report on progress towards establishing CORSIKA 8 as a flexible tool for this purpose, combining microscopic simulations of particle cascades with radio simulation and propagation capabilities for general inhomogeneous media. First, Section 2 gives an overview of the radio simulation modules available within CORSIKA 8, including both geometric-optics and full-electrodynamics approaches. Section 3 then shows example simulation results and highlights the complementarity of these tools, and Section 4 provides an outlook on future work.

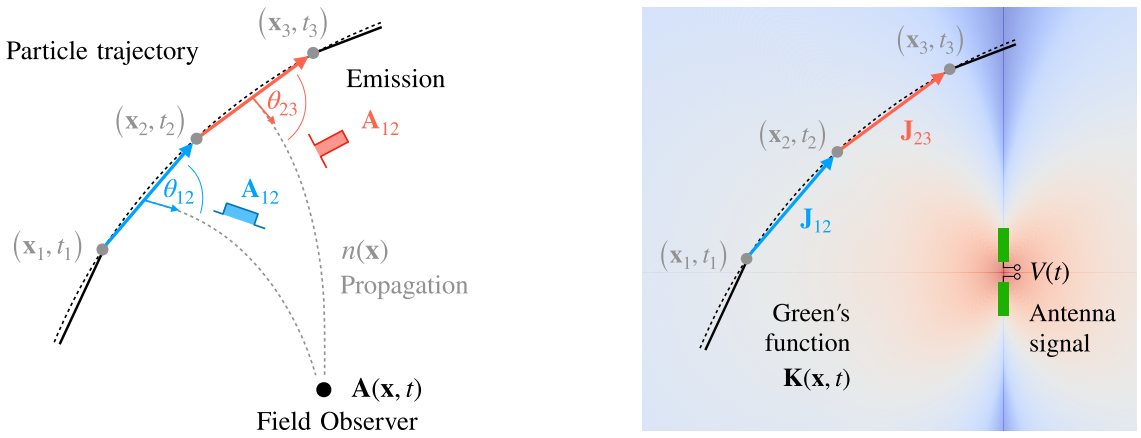

Figure 2: Left: Illustration of radio emission calculation with the *ZHS* algorithm, where contributions to the vector potential $\mathbf{A}$ from individual particle track segments are propagated to the observer location assuming geometric optics. Right: In the *Eisvogel* implementation, the antenna signal $V(t)$ resulting from a track segment is calculated by convolving the source current $\mathbf{J}$ with an electrodynamic Green's function $\mathbf{K}$, covering both emission and propagation.

2. Radio emission and propagation modeling in CORSIKA 8

CORSIKA 8 provides access to two different categories of radio emission- and propagation methods: an implementation of the widely-used *ZHS* [8] and *Endpoint* [9, 10] algorithms combined with straight-line or ray-traced radio propagation; and a new full-electrodynamics formulation provided by the *Eisvogel* package [11, 12]. Both are reviewed briefly below.

In the *ZHS* method (Fig. 2 left), the (possibly curved) trajectory of a charged particle is partitioned into a set of short straight track segments. The vector potential $\mathbf{A}_{ij}$ sourced by a track segment $i \to j$ is calculated analytically in the Fraunhofer limit, where it takes the simple form of a rectangular function whose duration and amplitude depend on the segment endpoints $(\mathbf{x}_i, t_i)$, $(\mathbf{x}_j, t_j)$ and the viewing angle θ_{ij}. (The track length is chosen to be sufficiently short such that the Fraunhofer limit applies.) Contributions from all track segments are then propagated to and accumulated at the observer location. Here, the short-wavelength limit of geometric optics is assumed, where radiation propagates along curved rays through an inhomogeneous refractive-index profile $n(\mathbf{x})$ and plane-wave Fresnel coefficients describe the transmission and reflection of rays at material boundaries. The geometric-optics limit is applicable provided that the medium through which the radiation propagates varies on length scales that are long relative to the wavelength. For example, for a frequency of $f = 400\,\mathrm{MHz}$, the wavelength is about $\lambda \sim 0.6\,\mathrm{m}$ in near-surface ice with a refractive index with $n = 1.3$. The *Endpoint* algorithm proceeds similarly, although the electric field $\mathbf{E}$ from a track segment is obtained directly from the change in velocity at the segment endpoints. Both approaches determine the electric field $\mathbf{E}$ at the location of the observer, which can subsequently be propagated through a model of the receiving antenna and signal-processing chain to determine the observed detector (voltage) signal $V(t)$.

If the medium contains inhomogeneities on the scale of the radiation wavelength, wave-optics phenomena become important and emission, propagation, and reception do not decouple. To cover this more-challenging situation, CORSIKA 8 interfaces to the external *Eisvogel* code. *Eisvogel*

uses the reciprocity properties of Maxwell's equations [13] to construct an electrodynamic Green's function $\mathbf{K}$ for the antenna signal $V(t)$. It is defined as the electric field distribution resulting in the medium if a source current corresponding to the impulse response of the signal chain is applied to the feed of the antenna. As such, the Green's function encodes a model of the antenna and its environment and may be calculated numerically for a general linear medium. During the cascade simulation (Fig. 2 right), each particle track segment is then interpreted as a line current element $\mathbf{J}$ and convolved with the Green's function, directly resulting in the contribution to the antenna signal $V(t)$ arising from the segment.

3. Example applications and discussion

To discuss the practical application of these methods, we consider situations representative of in-ice radio neutrino observatories. Realistic detector responses (where publicly available) are used to illustrate the typical use of CORSIKA 8 in an experimental setting.

3.1 In-ice particle cascades

In-ice radio neutrino observatories deploy antennas below the surface of the polar ice sheet, searching for Askaryan radiation emitted by neutrino-induced cascades in the ice. This radiation is coherent, and natural glacial ice is low-loss, making it possible to detect neutrino interactions several kilometers away from the antenna at energies $\gtrsim 10\,\mathrm{PeV}$. It is therefore critical to be able to precisely model the neutrino signature across a detector effective volume of the order of $10\,\mathrm{km}^3$. Previous work [14] verified that CORSIKA 8 is in near-perfect agreement with previous microscopic simulations using the ZHAireS [15] code for homogeneous ice. These ZHAireS results were also used to build fast parameterized models of in-ice Askaryan radiation that are heavily used in Monte Carlo simulations to study detector performance and sensitivity [16]. The study in Ref. [14] used a simple homogeneous ice model, representative of the deep bulk ice which contributes most to the neutrino effective volume.

In the following, we instead focus on in-ice cascades developing near the top of the ice sheet, where the inhomogeneous medium properties significantly affect the propagation of radiation. We select the refractive index of the ice to depend on the vertical coordinate z as

$$n(z) = \begin{cases} 1.000 & z \geq 0\,\mathrm{m}, \\ 1.780 - 0.454\,\exp\left[0.0202\,z/1\,\mathrm{m}\right] & z < 0\,\mathrm{m}, \end{cases} \tag{1}$$

where $z = 0\,\mathrm{m}$ marks the surface. No radial dependence is considered, i.e. the ice is assumed to be translation invariant in the plane parallel to the surface. In this model, as the ice compresses with increasing depth, the refractive index increases smoothly until it saturates at $n_{\mathrm{bulk}} \sim 1.780$ in the deep bulk ice. The parameterization in Eq. 1 applies to ice near the South Pole and has previously been used in the neutrino search of Ref. [17]. This "single-exponential" parameterization is widely used in situations where the absence of granular ice measurements prevents a more detailed characterization.

Fig. 3 shows the signal from a shower initiated by a vertically-downgoing electron at a depth of 2 m below the surface of the ice geometry of Eq. 1. The shower is observed by a vertically-polarized

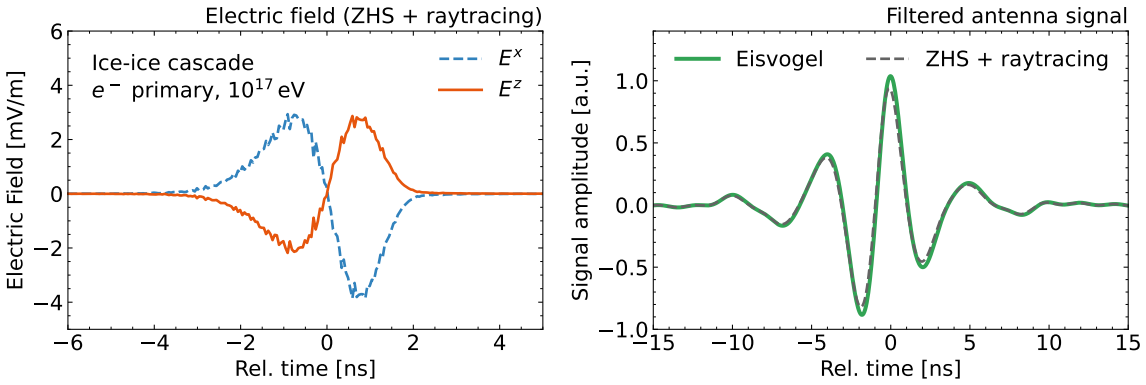

Figure 3: Simulation of the radio signal from an electron-induced particle cascade in the geometry described in the main text. Left: the cartesian electric field components E^x (horizontal) and E^z (vertical) calculated with the *ZHS* algorithm, propagated to the antenna using raytracing. The remaining field component E^y vanishes due to the symmetry of the situation and is not shown. Right: the antenna signal obtained by propagating the *ZHS* results through a model of the instrument response of Ref. [2], and compared to a direct calculation using *Eisvogel*.

dipole antenna at 100 m depth at a viewing direction $\sim 4°$ off the approximate in-ice Cherenkov angle. In the geometry of Eq. 1, the angle between the shower axis and the emission maximum is $\sim 41°$. The electric field is calculated with *ZHS* and ray-traced to the antenna, shown in Fig. 3 left. It displays the typical symmetric-bipolar shape of Askaryan radiation, polarized radially with respect to the shower axis. To simulate the signal observed in a realistic detector, the electric field is propagated through the instrumental response of the ARA-5 phased-array detector, available in Ref. [2]. The response has a passband of 150 MHz–720 MHz and a notch filter at 450 MHz to remove land mobile radio communications commonly used at South Pole station. A simple $1/f$ behavior was assumed for the effective height of the in-borehole dipole antenna. The resulting signal is shown in Fig. 3 right, where it is compared with the result from a full-electrodynamics calculation performed with *Eisvogel*. The agreement is near-perfect, indicating that geometric optics is sufficient to describe radiation propagation through this smoothly-inhomogeneous material distribution. Both radio algorithms, *Eisvogel* and *ZHS*, are run in parallel with the evolution of the cascade, ensuring that an identical set of particle tracks is used to compare the radio signals.

3.2 Ice-impacting air shower cores

Recent calculations [18] have shown that the dense cores of near-vertical air showers can impact the surface of the ice sheet and generate Askaryan radiation in the top 5–10 m of the ice sheet. Detection rates are estimated at 10–100 yr^{-1} [19] per detector station, larger than the expected neutrino rate by at least two orders of magnitude [20]. This illustrates the need for a thorough characterization of this background, complicated however by the fact that the near-surface ice shows seasonal variations and perturbations on the scale of 0.5 m [21], similar to the radiation wavelength in the passband of a typical detector.

Here, we study this challenging situation using *Eisvogel*. Fig. 4 (left) shows the refractive index profile extracted from ice density measurements performed near South Pole as part of the South Pole Ice Core (SPICEcore) project [22]. Non-smooth perturbations of the refractive index

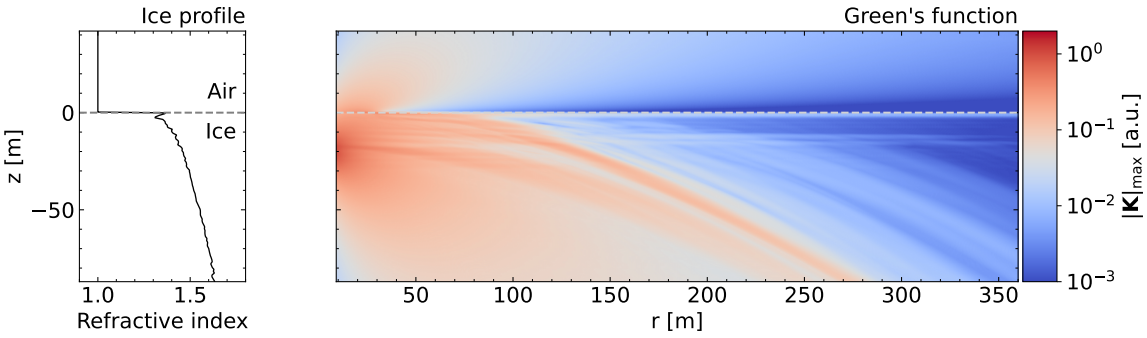

Figure 4: Left: Refractive index profile of near-surface ice as obtained from the South Pole Ice Core project [22]. Right: Illustration of the Green's function of an in-ice antenna at 20 m depth, calculated for this ice geometry. For visual clarity, the maximum magnitude of the Green's function $|\mathbf{K}|_{\max}(\mathbf{x}) = \max_t |\mathbf{K}|(\mathbf{x}, t)$ is shown.

of order 10% are clearly visible, superimposed on a smooth trend similar to the simple model in Eq. 1. Of note is also a density inversion just below the surface. Part of these fluctuations may be attributed to (systematic) uncertainties in the measurement. However, the reduction with depth of their magnitude combined with principled glaciological models [21], strongly suggest the presence of genuine non-smooth structure in the near-surface ice.

Using this material distribution, the Green's function $\mathbf{K}(\mathbf{x}, t)$ for a shallow receiver at 20 m depth is illustrated in Fig. 4 (right). *Eisvogel* interfaces with the open-source finite-difference time domain (FDTD) solver MEEP [23] to calculate the Green's function, exploiting its MPI capabilities to parallelize the computation over several processor cores. Importantly, this interaction remains hidden from the user, who only interacts with CORSIKA 8 in defining the environment geometry. The Green's function shows the characteristic ray-bending observed in the polar ice sheets, whereby radiation is refracted downwards in the refractive-index profile, creating a "shadowed" conical region with very low radiation intensity. Crucially, this effect is imperfect: density fluctuations in the ice can act as horizontal waveguides and efficiently carry radiation into the shadowed region. Conversely, a source located in this domain can produce a detectable signal in the receiver, as experimentally studied in Refs. [24, 25] and discussed below. This is a genuine wave-optics effect that lies outside the domain of applicability of geometric optics: For a smoothly-inhomogeneous ice profile, the boundary of the shadowed region forms a caustic that no ray can cross.

Fig. 5 (left) shows detector signals calculated for a vertical impacting air shower core initiated by a proton primary with an energy of 10^{17} eV. Here, the shower is captured by a detector array placed near the Cherenkov angle, leading to impulsive in-ice Askaryan signals being observed (cf. Fig. 3). The signal amplitude and spectral shape show the characteristic dependence on the viewing angle, with higher frequencies disappearing first as the receiver moves away from the Cherenkov cone. Fig. 5 (right) compares this situation to the case of an air shower core impacting the surface in the shadowed portion of the ice. The radiation signature changes completely in this regime, and instead of a nanosecond-pulse, the detector signal now takes on the character of a much longer (50–100 ns), dispersed waveform. This is the result of multipath propagation in the inhomogeneous ice, where radiation components are continuously reflected and refracted at the non-smooth ice inhomogeneities. Interestingly, this is qualitatively very similar to the event

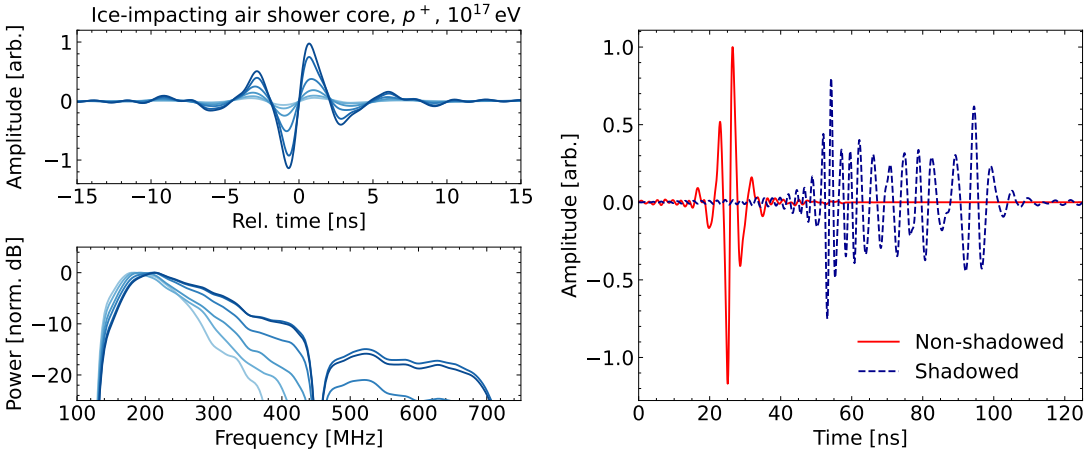

Figure 5: Left: Detector signals from a vertical air shower core impacting the ice, as observed in a number of in-ice receivers placed near the Cherenkov angle, shown in the time domain (top) and the frequency domain (bottom, normalized to peak power density). Darker colors indicate smaller angle differences relative to the Cherenkov angle. The same instrument response as in Fig. 3 is applied. Right: Comparison of detector signals for showers impacting in the "shadowed" (at $r = 250$ m) and "non-shadowed" (at $r = 25$ m, identical to the result on the left) portions of the ice surface. Both signals are separately normalized to visualize the signal shape differences; the relative amplitudes cannot be directly compared.

observed in the neutrino signal region of the analysis in Ref. [17], whose origin, thus far, has not been explained. It will be crucial to determine the rate of such events expected from impacting shower cores and to quantify the impact of this background on the design and sensitivity of neutrino searches.

4. Current status and outlook

CORSIKA 8 is evolving into a powerful framework to simulate radio emissions from particle showers in complex media. The code combines the ability to simulate cascades in general inhomogeneous media with a suite of different radio emission and propagation modules. These methods apply geometric optics as well as full-electrodynamics, together covering a range of scenarios applicable to most (if not all) radio particle detection experiments. Already now, CORSIKA 8 enables the expert user to investigate challenging situations significantly beyond the capabilities of previous simulation frameworks. For in-ice neutrino observatories, this includes studying the radiation signature of sources in the geometrically-shadowed portion of the ice, such as from impacting air shower cores or neutrinos interacting near the caustic. Situations of similar complexity exist in other contexts, from the detection of upgoing or emerging showers in non-flat terrain [26] to the exploration of the moon [3]. The generality of CORSIKA 8 and its radio propagation methods makes the framework immediately applicable also to these scenarios.

Continued development, extension, and validation of the code is in progress. We expect that in-ice neutrino observatories with their complicated detector environment will serve as a near-term testbed for the capabilities of these methods and that they will provide the datasets to validate their results. The emphasis of future work will be to also make these tools readily accessible to the

general user and the wider radio particle detection community, and to extend them to also apply to anisotropic media.

References

[1] **RNO-G** Collaboration, S. Agarwal *et al.* *JINST* **20** (2025) P04015.
[2] **ARA** Collaboration, P. Allison *et al.* *Nucl. Instrum. Meth. A* **930** (2019) 112–125.
[3] E. S. Costello, R. R. Ghent, A. Romero-Wolf, *et al.* *Geophysical Research Letters* **52** no. 6, .
[4] S.-H. Wang, J. Nam, P. Chen, *et al.* *JCAP* **11** (2022) 022.
[5] **BEACON** Collaboration, D. Southall, C. Deaconu, V. Decoene, *et al.* *Nucl. Instrum. Meth. A* **1048** (2023) 167889.
[6] **GRAND** Collaboration, J. Álvarez-Muñiz, R. A. Batista, A. Balagopal V., *et al.* *Science China Physics, Mechanics, and Astronomy* **63** no. 1, (2020) 219501.
[7] P. W. Gorham, J. Bynes, B. Fox, *et al.* *Phys. Rev. Accel. Beams* **21** (2018) 072901.
[8] J. Alvarez-Muñiz, A. Romero-Wolf, and E. Zas *Phys. Rev. D* **81** (2010) 123009.
[9] T. Huege, M. Ludwig, and C. James *AIP Conf. Proc.* **1535** (2013) 128–132.
[10] J. Alameddine, J. Albrecht, J. Ammerman-Yebra, *et al.* *Astroparticle Physics* **166** (2025) 103072.
[11] P. Windischhofer, C. Welling, and C. Deaconu *PoS* **ICRC2023** (2023) 1157.
[12] P. Windischhofer, C. Deaconu, and C. Welling *PoS* **ARENA2024** (2024) 051.
[13] W. Riegler and P. Windischhofer *Nucl. Instrum. Meth. A* **980** (2020) 164471.
[14] M. Durán de las Heras, "Askaryan Radio Emission with CORSIKA8." `https://urn.kb.se/resolve?urn=urn:nbn:se:uu:diva-538021`.
[15] J. Alvarez-Muñiz, A. Romero-Wolf, and E. Zas *Phys. Rev. D* **81** (2010) 123009.
[16] C. Glaser, D. García-Fernández, A. Nelles, *et al.* *The European Physical Journal C* **80** no. 2, (2020) 77.
[17] **ARA** Collaboration, P. Allison *et al.* *Phys. Rev. D* **105** (2022) 122006.
[18] S. De Kockere, K. de Vries, N. van Eijndhoven, and U. Latif *Phys. Rev. D* **106** no. 4, (2022) .
[19] A. Coleman, C. Glaser, R. Rice-Smith, *et al.* *Astroparticle Physics* **172** (2025) 103136.
[20] V. Valera, M. Bustamante, and C. Glaser *Phys. Rev. D* **107** (2023) 043019.
[21] M. C. Stevens, V. Verjans, J. M. D. Lundin, *et al.* *Geosci. Model Dev.* **13** no. 9, (2020) .
[22] K. Casey, T. Fudge, T. Neumann, and E. Steig *Annals of Glaciology* **55** (2014) 137–146.
[23] A. F. Oskooi, D. Roundy, M. Ibanescu, *et al.* *Computer Physics Communications* **181** no. 3, (2010) 687–702.
[24] C. Deaconu, A. G. Vieregg, S. A. Wissel, *et al.* *Phys. Rev. D* **98** no. 043010, (2018) .
[25] S. W. Barwick, E. C. Berg, D. Z. Besson, *et al.* *JCAP* **07** no. 55, (2018) .
[26] **TAMBO** Collaboration, W. Thompson *PoS* **ICRC2023** (2023) 1109.

The CORSIKA 8 Collaboration

J.M. Alameddine[1,2], J. Albrecht[1,2], A.A. Alves Jr.[3,4], J. Ammerman-Yebra[5], L. Arrabito[6], D. Baack[1,2], R. Cesista[6], A. Coleman[7], C. Deaconu[8], H. Dembinski[1,2], D. Elsässer[1,2], R. Engel[3], A. Faure[6], A. Ferrari[3], C. Gaudu[9], C. Glaser[7,1], M. Gottowik[3], D. Heck[3], T. Huege[3,10], K.H. Kampert[9], N. Karastathis[3], L. Nellen[11], D. Parello[12,13], T. Pierog[3], R. Prechelt[14], M. Reininghaus[15], W. Rhode[1,2], F. Riehn[1], M. Sackel[1,2], P. Sampathkumar[3], A. Sandrock[9], J. Soedingrekso[1,2], R. Ulrich[3], P. Windischhofer[8], B. Yue[9]

[1] Technische Universität Dortmund (TU), Department of Physics, Dortmund, Germany
[2] Lamarr Institute for Machine Learning and Artificial Intelligence, Dortmund, Germany
[3] Karlsruhe Institute of Technology (KIT), Institute for Astroparticle Physics (IAP), Karlsruhe, Germany
[4] University of Cincinnati, Cincinnati, OH, United States
[5] IMAPP, Radboud University Nijmegen, Nijmegen, The Netherlands
[6] Laboratoire Univers & Particules de Montpellier, CNRS & Université de Montpellier (UMR-5299), 34095 Montpellier, France
[7] Uppsala University, Department of Physics and Astronomy, Uppsala, Sweden
[8] Department of Physics, Enrico Fermi Institute, Kavli Institute for Cosmological Physics, University of Chicago, Chicago, IL 60637, USA
[9] Bergische Universität Wuppertal, Department of Physics, Wuppertal, Germany
[10] Vrije Universiteit Brussel, Astrophysical Institute, Brussels, Belgium
[11] Universidad Nacional Autónoma de México (UNAM), Instituto de Ciencias Nucleares, México, México
[12] DALI, Univ Perpignan, Perpignan, France
[13] LIRMM Univ Montpellier, CNRS, Montpellier, France
[14] University of Hawai'i at Manoa, Department of Physics and Astronomy, Honolulu, USA
[15] Independent researcher

PoS(ICRC2025)1214

Acknowledgements

We thank T. Sjöstrand, L. Lönnblad, and the Pythia 8 collaborators for their support in the implementation of Pythia 8/Angantyr in CORSIKA 8.

This research was funded by the Deutsche Forschungsgemeinschaft (DFG, German Research Foundation) – Projektnummer 445154105 and Collaborative Research Center SFB1491 "Cosmic Interacting Matters - From Source to Signal". This research has been partially funded by the Federal Ministry of Education and research of Germany and the state of North Rhine-Westphalia as part of the Lamarr Institute for Machine Learning and Artificial Intelligence. We acknowledge support through project UNAM-PAPIIT IN114924.

This work has also received financial support from Ministerio de Ciencia e Innovación/Agencia Estatal de Investigación (PRE2020-092276). A. Coleman is supported by the Swedish Research Council (Vetenskapsrådet) under project no. 2021-05449. C. Glaser is supported by the Swedish Research Council (Vetenskapsrådet) under project no. 2021-05449 and the European Union. F. Riehn received funding from the European Union's Horizon 2020 research and innovation programme under the Marie Skłodowska-Curie grant agreement No. 101065027. P. Windischhofer and C. Deaconu thank the NSF for Award 2411662. The authors acknowledge support by the High Performance and Cloud Computing Group at the Zentrum für Datenverarbeitung of the University of Tübingen, the state of Baden-Württemberg through bwHPC and the German Research Foundation (DFG) through grant no INST 37/935-1 FUGG. The computations were partially carried out on the PLEIADES cluster at the University of Wuppertal, which was supported by the Deutsche Forschungsgemeinschaft (DFG, grant No. INST 218/78-1 FUGG) and the Bundesministerium für Bildung und Forschung (BMBF).